Repair of Damaged Parts Using Wire Arc Additive Manufacturing In Machine Tools Remanufacturing

Jeong-Hak Lee
Changwon National University
Choon Man Lee (cmlee@changwon.ac.kr)
Changwon National University
Dong-Hyeon Kim
Changwon National University

Research Article

Keywords: Wire arc additive manufacturing, Remanufacturing, Repair, Lathe cross slide, Gray cast iron

Posted Date: July 8th, 2021

DOI: https://doi.org/10.21203/rs.3.rs-637275/v1

Abstract

Mechanical parts manufactured using additive manufacturing (AM) processes are used in various fields, such as the aerospace, automobile, and machine tool fields. Recently, many researchers have been actively researching AM processes, owing to their advantages in fabricating complex-shaped components that are difficult to process using conventional processes such as rolling, forging, and casting. One of the AM processes, wire arc additive manufacturing (WAAM), is widely used for manufacturing and repair. Mechanical parts usually suffer from severe damage, such as wear and cracks, during operation. Therefore, research on the damaged parts is often required for repairs. This study was performed to investigate the repair of damaged parts using WAAM in machine tool remanufacturing. In general, these parts are often damaged owing to falls of the workpieces and the inexperience of workers; the cross slide is one of the parts damaged most often in a lathe. Accordingly, this study used the cross slide as an example. First, the damaged area was partially cut flat. Second, it was filled with a metal wire using WAAM. Third, post-processing was performed to adjust the surface quality and shape accuracy. Then, the microstructure, chemical composition, and mechanical property of the repaired part were analyzed. Finally, the repaired cross slide was used to replace damaged parts. In general, this method can be applied to various mechanical parts such as impellers, turbine blades, and machine tools.

Introduction

Additive manufacturing (AM) can be used to produce parts with complicated geometric features, or to partially repair damaged parts. AM is an efficient and economical process for reducing material waste. Recently, many metallic parts have been manufactured using AM. AM processes can be classified into two types: powder bed fusion (PBF), and direct energy deposition (DED). PBF manufactures parts by selectively irradiating high-power energy against a bed on which a metal powder is spread. DED directly deposits metal powders or wires region-by-region [1–6]. PBF is mostly suitable for complex metal parts where dimensional accuracy and surface quality are concerns, owing to it capabilities in manufacturing near-net shapes with post-processing requirements by means of secondary machining operations. The product quality of objects manufactured using PBF has been observed as better than that of objects deposited using DED. However, it is difficult to achieve high-efficiency manufacturing using PBF. The material usage in DED is very efficient in situations where only the required amount of material is deposited onto the build platform. DED is generally faster than PBF and is well-suited for the manufacturing of large structures. Moreover, DED can be used to refurbish existing parts [7–11].

WAAM is a DED approach that enables the production of three-dimensional components in a layer-wise manner [12]. WAAM has been recognized as an effective solution for part repair owing to its low material usage, high deposition rates, and good structural quality. The deposition rates are sufficiently high to allow for the rapid manufacturing of large-scale parts [13–17]. This method is similar to welding, and can be used to deposit materials on existing products; thus, it is available for repair purposes. In addition,

because AM using multiple materials is possible in DED, various alloys and composites can be manufactured using various metal materials [18].

Generally, there are two types of defects: structural defects, and morphological defects. Structural defects include slips, point defects, and lattice defects. This study only considers with morphological defects, which typically include holes, cracks, surface marks, and notches. Oh et al. [1] verified the applicability of DED to repairing damaged PBF parts. Onuike et al. [19] investigated the effectiveness of two slots with different geometric shapes (rectangular and trapezoidal) in repairing internal cracks, aiming to understand the influence of the deposition orientation on the mechanical properties of the repaired components. Sun et al. [20] studied fatigue behaviors after deposition using materials different from those in a substrate. Li et al. [21] proposed a geometry for a concave groove part according to the shape of a deposition bead during repair using WAAM. Poonnayom et al. [22] investigated a shield metal arc welding process for producing a hard face. Li et al. [23] studied the surface remanufacturing of materials using metal powder. Li et al. determined the residual stress, cracking sensitivity, and mechanical properties during a laser remanufacturing process for ductile iron.. Balit et al. [24] studied self-heating behaviors during the cyclic loading of stainless steel specimens repaired by DED. Jim et al. [25] investigated the remanufacture of hot forging dies, aiming to improve the performance. Wilson et al. [26] proposed environmental benefits from remanufacturing and repairing high-value engineering components using AM.

In this study, the damaged parts of a cross slide were repaired using WAAM in machine tool remanufacturing. The cross slide was manufactured from gray cast iron, and nickel wire was used as the deposition material in the WAAM for repair. A material different from that of the substrate was used for the repair in the WAAM. The microstructure, chemical composition, and mechanical property of the repaired parts were evaluated and analyzed.

Machine Tool Remanufacturing

As restrictions on the environment have been tightened, the concept of remanufacturing has become more important. Machine tools are a common subject of remanufacturing. There are many old machine tools discarded every year, and the disposal of machine tools causes environmental pollution owing to the waste of resources and/or incineration. Figure 1 shows the life cycle of a product for remanufacturing. Remanufacturing is a return from the management stage to the product manufacturing stage, rather than incineration. The remanufacturing stage refers to repair of damaged parts. It can reduce the waste of resources and minimize the environmental pollution caused by incineration. This study concerns the remanufacturing stage in the life cycle of a product.

Materials And Method

3.1 Materials

The gray cast iron (International Standards Organization (ISO)) 185/JL/250 with 39.5 *mm* was used as the substrate in these experiments. Generally, the gray cast iron ISO 185/JL/250 has a tensile strength between 250 *MPa* and 300 *MPa*. The specifications for the damaged parts were proposed as 10 *mm* in width and 5 *mm* in height. The test specimens were designed according to the specifications. Figure 2 shows the specifications of the test specimens.

The metal wire used for repair was American Welding Society A5.14 ERNi-1. A metal wire with 1.2Φ was used as the deposition material. The substrate and metal wires are shown in Table 1.

In WAAM, it is important to prevent defects such as porosity and cracks in the repaired parts. In general, gray cast iron can easily form pores and cracks when the amount of input heat increases. The substrate generally contains a large amount of carbon. The substrate cracks owing to the heat caused by deposition at room temperature. When welding gray cast iron, a large amount of heat input causes a high risk of cracks, owing to temperature differences during cooling. Nickel, which is used as a deposition material, is combined with the substrate to improve the wear resistance. In addition, cracks are restrained through graphitization in the process of combination with the gray cast iron. Therefore, the gray cast iron is repaired using a material different from that of the substrate. A metal wire containing nickel is suitable as a deposition material for gray cast iron with a high carbon content.

Table 1
Chemical composition (wt%)

Substrate									
C		Si		Mn	P	S		Fe	
3.166		1.838		0.612	0.042	0.027		Bal.	
Metal wire									
Ni	Ti	Si	Mn	Al	Fe	Cu	P	C	S
96.09	2.57	0.35	0.35	0.29	0.04	0.01	0.003	0.002	0.001

3.2 Method

In this study, the deposition path was a zigzag path in preliminary experiments. This method was used to minimize the differences in the deposition height. Figure 3 shows the deposition path used in the preliminary experiments for the determination of the deposition parameters. The purpose of the preliminary experiments was to determine the parameters for ensuring that the metal wires were completely molten and no spatters occurred. Table. 2 shows the deposition parameters. In addition, the test specimens were repaired using these parameters. The parameters included the current (I), voltage (V), wire feed speed (F_{wire}), travel speed (S), and gas flow rate. The gas flow rate was maintained at 20 L/min.

Table 2
Deposition parameters

No	I (A)	V (V)	F_{wire} (m/min)	S (mm/s)
1	100	12.2	2.6	5
2	100	12.2	2.6	6
3	180	14.6	5.2	5
4	180	14.6	5.2	6
5	260	16.5	8.2	5
6	260	16.5	8.2	6

The zigzag method was applied to the cross slide. A cross slide, one of the main components of a lathe, was repaired as a remanufactured product. Cross slides are used often, and play a role in transporting tool posts. However, cross slides are frequently damaged owing to the inexperience of workers and falling of workpieces. In a worksite, a damaged cross slide is often used for grinding, or as-is. In such cases, processing errors may occur when a damaged cross slide is used. Therefore, it is necessary to repair damaged parts.

WAAM is advantageous for repairing large workpieces and has high productivity, owing to its rapid deposition speed. Therefore, in this study, a cross slide with defects such as fractures, abrasions, cracks, and holes was repaired using WAAM. Figure 4 shows an example of the structure of the lathe, along with the parts of the lathe requiring repair.

3.3 Experimental setup

Fig. 5 shows the principles of the WAAM and equipment used for these deposition experiments. The ABB IRB 6700 industrial robot was used in the WAAM. The robot had a payload of approximately 200 , and the travel speeds were determined. The TPS 500i welding machine is a metal inert gas(MIG) type machine with cold metal transfer(CMT) functionality made by Fronius. Argon gas and metal wire were supplied to the inside of the welding torch through the welding machine. The welding machine controlled the current, voltage, and wire feed speeds.

Results And Discussion

4.1 Preliminary experiments for deposition conditions

The current and travel speeds were determined as the deposition parameters. The currents were 100 *A*, 180 *A*, and 260 *A*, and the travel speeds were 5 *mm/s* and 6 *mm/s*, respectively. Figure 6 shows the results from the preliminary experiments for determining the parameters. At a current of 100 A , the deposition parameters are unsuitable regardless of the travel speed, as shown in Fig. 6a and b. In this

case, the amount of wire supplied is insufficient. In addition, the wire feed speed is too low, so the deposition beads do not overlap in the zigzag method. This means that the relationship between the metal wire used in the deposition and parameters is not appropriate. The metal wire is completely molten owing to a suitable current at 180 A regardless of the travel speed, as shown in Fig. 6c and d. When the current is 180 A, the spatter depends on the travel speed, as shown in Fig. 6c. The spatter occurs only at 5 mm/s, i.e., a slow deposition speed, indicating the formation of excessive melting pools and increased heat inputs, thereby resulting in spatters. When the travel speed is 6 mm/s, the deposition speed is adequate. Therefore, in this case, spatters are not caused by this parameter. When the current is 260 A, the metal wire is completely molten, as shown in Fig. 6e and f. However, spatter occurs. This is because the wire feed speed is too high, and the current is high. Through experiments to determine the parameters, the best deposition parameters are as follows: the current (*I*), voltage (*V*), wire feed speed (F_{wire}), and travel speed (*S*) are 180 A, 14.6 V, 5.2 *m/min*, and 6 mm/s, respectively. Table 3 presents the results of the preliminary experiments based on the deposition parameters. The deposition beads do not overlap in the zig-zag method at 100 A. Therefore, the case when the current is 100 A is excluded from the experiments with test specimens. Ultimately, the conditions used in the repair experiments were 180 A and 260 A, respectively.

Thus, experiments with the test specimens were performed under the determined conditions. Figure 7 shows the repaired test specimens. Figure 7a and b show the results of experiments at 180 A and 260 A, respectively, at the same travel speed of 6 mm/s. When the current is 260 A, many spatters occur. When the current is 180A, it is possible to verify that the wires are completely molten without spatter formation. Therefore, this is considered the most suitable parameter value for the current.

Table 3
Results of preliminary experiments

No	*I* (A)	*V* (V)	F_{wire} (m/min)	*S* (mm/s)	Spatter	Overlap	Class
a	100	12.2	2.6	5	×	△	Normal
b	100	12.2	2.6	6	×	×	Bad
c	180	14.6	5.2	5	△	●	Normal
d	180	14.6	5.2	6	×	●	Good
e	260	16.5	8.2	5	●	●	Bad
f	260	16.5	8.2	6	△	●	Normal

4.2 Mechanical property and microstructure

After performing preliminary experiments, the deposition cross-sections were confirmed for the cases with 180 *A* and 260 *A*, where the wire was completely molten. Figure 8 shows the digital microscopy results from the preliminary experiments for parameter determination. The pores occur under both 180 *A* and

260 *A*, but the pores occur less often at 180*A* than at 260 *A*. Repairs were performed on the test specimens with the two determined parameters.

The mechanical property, microstructure, and chemical composition of the repaired specimens were analyzed. Figure 9 shows the results of a digital microscope analysis of the cross-sections of the repaired specimen. Porosity occurs more often when there is a large amount of heat input. The sizes of the pores are also large under conditions with a high heat input (i.e., of 260 *A)*.

Figure 10 shows the results regarding the microstructure and chemical composition. Figure 10a and b show the results regarding the microstructure and chemical composition of the test specimen repaired using WAAM when the currents are 180 *A* and 260 *A*, respectively. A comparison of Fig. 10a and b shows that micro-pores occur in the substrate when the current is 260 *A*. The Ni value change from 96.09–70.24% among the chemical components of the wire when the current is 180 *A*. Fe, one of the chemical components of the substrate, changes from 94.32–91.59% when the current is 180 *A*. In addition, Ni changes from 96.09–70.78% among the chemical components of the wire when the current is 260 *A*. Fe changes from 94.32–91.3% when the current is 260 *A*.

Figure 11 shows the results from the Vickers hardness measurements. Generally, the hardness is higher in the deposition zone than in the substrate. In addition, the hardness increases as the nickel content increases. The hardness gradually increases as the substrate and nickel are combined at the interface, and the hardness is the highest in the deposition zone. However, there is little difference in the hardness between the deposition zone and substrate. The hardness shows a 17% increase in the repaired specimen at 180 *A* relative to the gray cast iron. Moreover, the hardness shows a 15% increase in the repaired specimen at 260 *A* relative to the gray cast iron. Thus, the hardness values of test specimens repaired at 180 *A* and 260 *A* are not significantly different.

4.3 Verification experiment

A verification experiment was performed based on experimental results. Figure 12 shows a schematic of the specimen for verification. The specimens for the verification experiment were produced in parts of the cross slide where breakage occurred frequently. Figure 13 shows the workflow of the repair of the damaged part with surface defects using machining and WAAM. The surface was flattened through slot machining to ensure that the deposition material was well-bonded to the surface. In addition, slot machining was applied to make the deposition height approximately constant. The surface flattened through slot processing was filled with the deposition material using WAAM. Post-processing was then performed to obtain the same specifications as the existing parts. The verification experiment was performed at 180 A, owing to the sizes of the pores and mechanical property. Figure 14 shows the results of the verification experiment.

Conclusion

This study examined the repair of damaged parts of a cross slide using WAAM. The repair procedure can be divided into three parts: (i) partial machining, (ii) WAAM, and (iii) post-processing. The conclusions are summarized as follows.

1) It was necessary to partially cut the surface flat so that the deposition materials can be effectively combined in damaged areas. In addition, similar deposition heights could be obtained by using the zigzag method on a flat surface. Nickel wires were used as deposition materials to suppress cracks and pores in the WAAM.

2) The cross slide was repaired by filling the damaged area with deposition materials using WAAM. The microstructure, chemical composition, and mechanical property of the repaired specimens were analyzed under conditions of 180 *A* and 260 *A*. The substrate showed graphite flakes, characteristic of gray cast iron; micropores were found at the interfaces of specimens repaired at 260 *A*. In the deposition zone, the deposition material was well-deposited, without micropores. The chemical compositions of the repaired specimens at 260 *A* and 180 *A* were not significantly different. The hardness of the specimen repaired at 180 *A* increased by 17% compared to the gray cast iron; the hardness of the specimen repaired at 260 *A* was 15% higher than that of the gray cast iron.

3) The damaged parts were repaired using WAAM. Post-processing was essential for adjusting the specifications of the original parts after AM. The post-processing allowed for high precision in the deposition area. A specimen was repaired for verification, based on the shape of the cross slide. Post-processing of the repaired specimen was performed with the same specifications as those for the original parts. Finally, the repair was successfully carried out on the original parts.

In this study, the repair of machine tool parts made of gray cast iron was successfully conducted using WAAM with nickel wire. Machine tools have various parts made of gray cast iron, e.g., cross slides, beds, and headstock bodies. The results of this study can be applied to various such parts, as well as to machine tools.

Declarations

Author contributions Jeong-Hak Lee: Experiments, Analyses, Measurements, and Writing-Original draft preparation. Dong-Hyeon Kim: Investigation, Writing-Reviewing, Editing, and Supervision. Choom-Man Lee: Project administration, Writing-Reviewing, Editing and Supervision.

Funding This work was supported by the Korea Institute of Energy Technology Evaluation and Planning(KETEP) and the Ministry of Trade, Industry & Energy(MOTIE) of the Republic of Korea [No. 20206310100040] and the National Research Foundation of Korea (NRF) grant funded by the Korea government (MSIT) [No. 2019R1A5A8083201].

Data availability The datasets used or analyzed during the current study are available from the corresponding author on reasonable request.

Ethics approval This paper is our original unpublished work, and it has not been submitted to any other journal for review.

Consent to participate All authors were fully involved in the study and preparation of the manuscript, and each of the authors has read and concurs with the content in the final manuscript.

Consent for publication All suthors consent to publish the content in the final manuscript.

Competing interests The authors declared no competing interests.

References

1. Oh WJ, Lee WJ, Kim MS et al (2019) Repairing additive-manufactured 316L stainless steel using direct energy deposition. Opt Laser Technol 117:6–17. https://doi.org/10.1016/j.optlastec.2019.04.012
2. Ahn DG (2021) Directed Energy Deposition (DED) Process: State of the Art. Int J Precis Eng Manuf - Green Technol 8:703–742. https://doi.org/10.1007/s40684-020-00302-7
3. Saboori A, Aversa A, Marchese G, Biamino S (2019) Application of Directed Energy Deposition-Based Additive Manufacturing in Repair. Appl Sci 9:3316. https://doi.org/10.3390/app9163316
4. Takagi H, Sasahara H, Abe T et al (2018) Material-property evaluation of magnesium alloys fabricated using wire-and-arc-based additive manufacturing. Addit Manuf 24:498–507. https://doi.org/10.1016/j.addma.2018.10.026
5. Kim DH, Kim TJY, Wang X et al (2018) Smart Machining Process Using Machine Learning: A Review and Perspective on Machining Industry. Int J Precis Eng Manuf - Green Technol 5:555–568. https://doi.org/10.1007/s40684-018-0057-y
6. Jiménez A, Bidare P, Hassanin H et al (2021) Powder-based laser hybrid additive manufacturing of metals: a review. Int J Adv Manuf Technol 114:63–96. https://doi.org/10.1007/s00170-021-06855-4
7. Paolini A, Kollmannsberger S, Rank E (2019) Additive manufacturing in construction: A review on processes, applications, and digital planning methods. Addit Manuf 30:100894. https://doi.org/10.1016/j.addma.2019.100894
8. Yan L, Chen Y, Liou F (2020) Additive manufacturing of functionally graded metallic materials using laser metal deposition. Addit Manuf 31:100901. https://doi.org/10.1016/j.addma.2019.100901
9. Akbari M, Kovacevic R (2018) An investigation on mechanical and microstructural properties of 316LSi parts fabricated by a robotized laser/wire direct metal deposition system. Addit Manuf 23:487–497. https://doi.org/10.1016/j.addma.2018.08.031
10. Kim H, Cha M, Kim BC et al (2019) Maintenance Framework for Repairing Partially Damaged Parts Using 3D Printing. Int J Precis Eng Manuf 20:1451–1464. https://doi.org/10.1007/s12541-019-00132-x

11. Pal S, Gubeljak N, Bončina T et al (2021) The effects of locations on the build tray on the quality of specimens in powder bed additive manufacturing. Int J Adv Manuf Technol 112:1159–1170. https://doi.org/10.1007/s00170-020-06563-5
12. Campatelli G, Montevecchi F, Venturini G et al (2020) Integrated WAAM-Subtractive Versus Pure Subtractive Manufacturing Approaches: An Energy Efficiency Comparison. Int J Precis Eng Manuf - Green Technol 7:1–11. https://doi.org/10.1007/s40684-019-00071-y
13. Williams SW, Martina F, Addison AC et al (2016) Wire + Arc Additive Manufacturing. Mater Sci Technol 7:641–647. https://doi.org/10.1179/1743284715Y.0000000073
14. Rodrigues TA, Duarte V, Miranda RM et al (2019) Current Status and Perspectives on Wire and Arc Additive Manufacturing (WAAM). Materials 12:1121. https://doi.org/10.3390/ma12071121
15. Cunningham CR, Flynn JM, Shokrani A et al (2018) Invited review article: Strategies and processes for high quality wire arc additive manufacturing. Addit Manuf 22:672–686. https://doi.org/10.1016/j.addma.2018.06.020
16. Dinovitzer M, Chen X, Laliberte J et al (2019) Effect of wire and arc additive manufacturing (WAAM) process parameters on bead geometry and microstructure. Addit Manuf 26:138–146. https://doi.org/10.1016/j.addma.2018.12.013
17. Zeng Z, Cong BQ, Oliveira JP et al (2020) Wire and arc additive manufacturing of a Ni-rich NiTi shape memory alloy: Microstructure and mechanical properties. Addit Manuf 32:101051. https://doi.org/10.1016/j.addma.2020.101051
18. Woo WS, Kim EJ, Jeong HI, Lee CM (2020) Laser-Assisted Machining of Ti-6Al-4V Fabricated by DED Additive Manufacturing. Int J Precis Eng Manuf - Green Technol 7:559–572. https://doi.org/10.1007/s40684-020-00221-7
19. Onuike B, Bandyopadhyay A (2019) Additive manufacturing in repair: Influence of processing parameters on properties of Inconel 718. Mater Lett 252:256–259. https://doi.org/10.1016/j.matlet.2019.05.114
20. Sun S, Da, Liu Q, Brandt M et al (2014) Effect of laser clad repair on the fatigue behaviour of ultra-high strength AISI 4340 steel. Mater Sci Eng A 606:46–57. https://doi.org/10.1016/j.msea.2014.03.077
21. Li Y, Han Q, Horváth I, Zhang G (2019) Repairing surface defects of metal parts by groove machining and wire + arc based filling. J Mater Process Tech 274:116268. https://doi.org/10.1016/j.jmatprotec.2019.116268
22. Poonnayom P, Kimapong K (2018) SMAW electrodes selection for producing hard-faced layer on FC25 cast iron surface. Key Eng Mater 777 KEM:339–343. https://doi.org/10.4028/www.scientific.net/KEM.777.339
23. Li Y, Dong S, Yan S et al (2018) Surface remanufacturing of ductile cast iron by laser cladding Ni-Cu alloy coatings. Surf Coatings Technol 347:20–28. https://doi.org/10.1016/j.surfcoat.2018.04.065
24. Balit Y, Joly L, Szmytka F et al (2020) Materials Science & Engineering A Self-heating behavior during cyclic loadings of 316L stainless steel specimens manufactured or repaired by Directed Energy

Deposition. Mater Sci Eng A 786:139476. https://doi.org/10.1016/j.msea.2020.139476

25. Jim F, Crawford C et al (2019) Remanufacture of hot forging tools and dies using laser metal deposition with powder and a hard-facing alloy. J Remanufacturing 9:189–203. https://doi.org/10.1007/s13243-018-0063-9
26. Wilson JM, Piya C, Shin YC et al (2014) Remanufacturing of turbine blades by laser direct deposition with its energy and environmental impact analysis. J Clean Prod 80:170–178. https://doi.org/10.1016/j.jclepro.2014.05.084

Figures

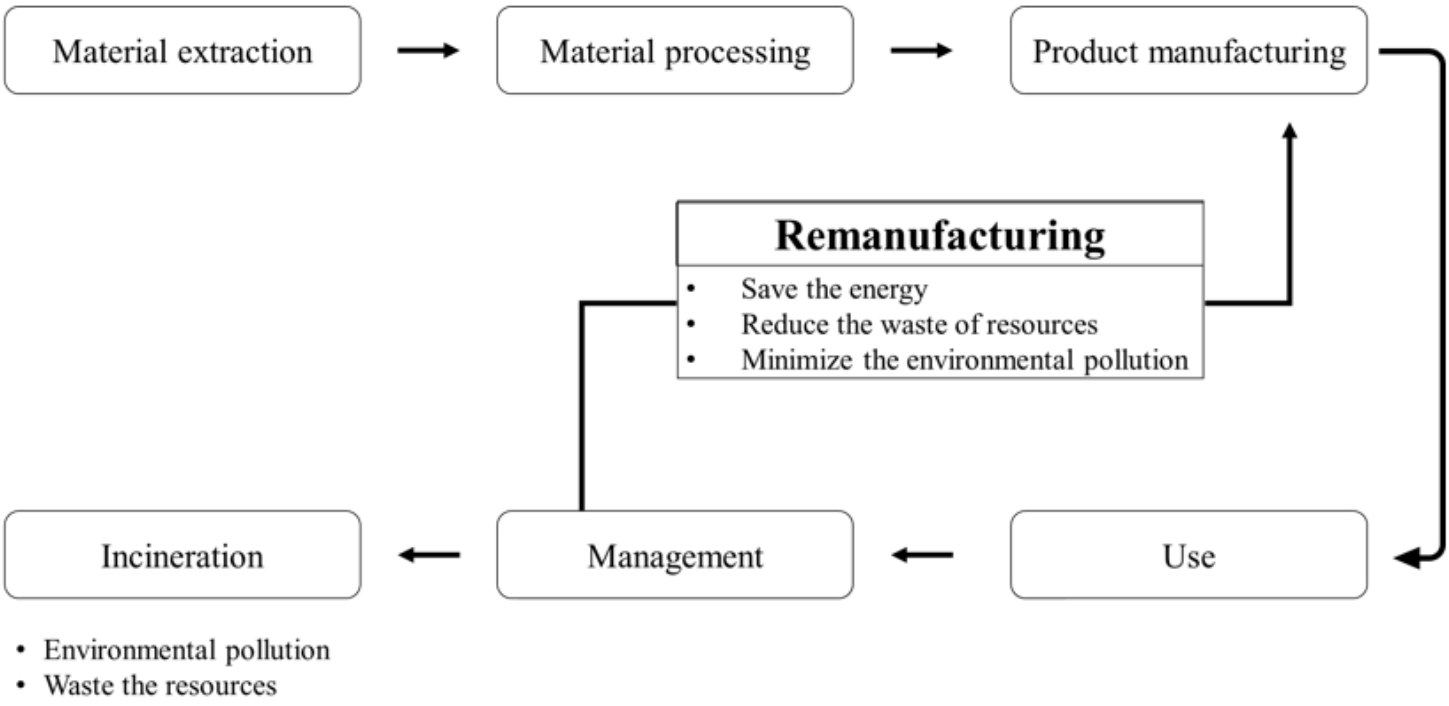

Figure 1

Life cycle of a product for remanufacturing

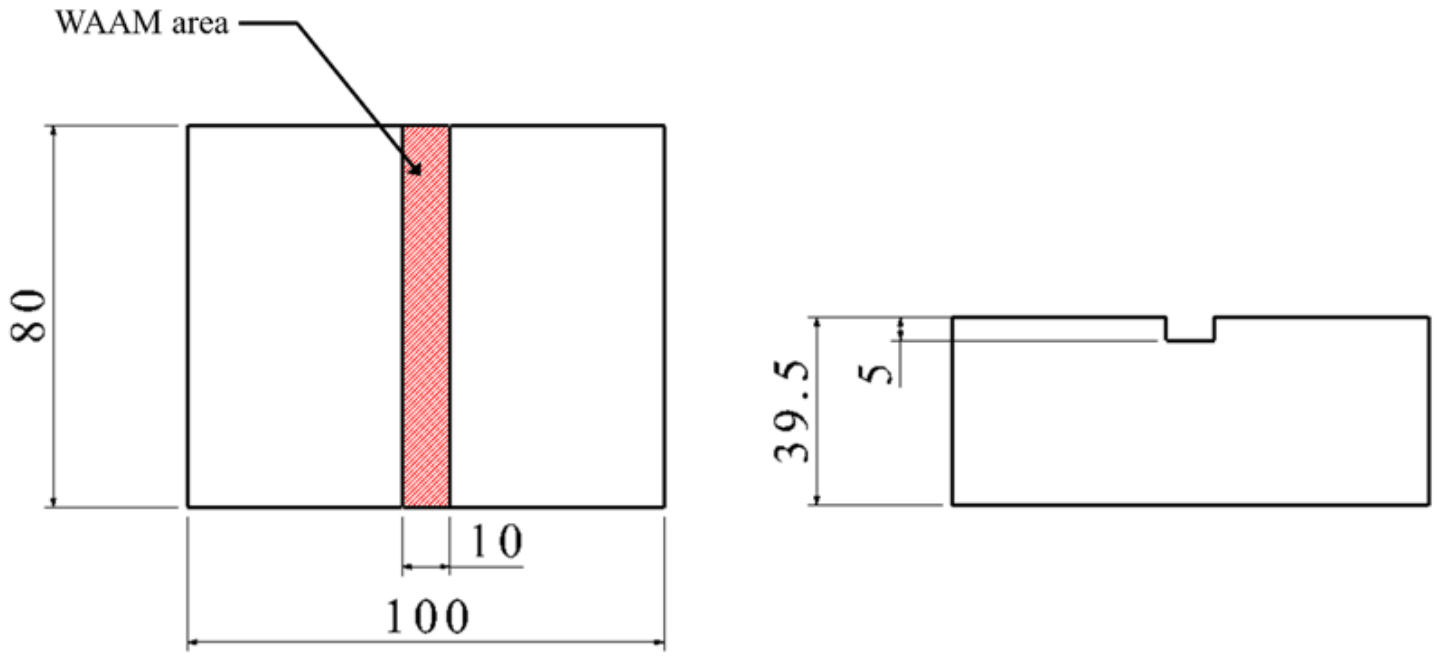

Figure 2

Specification of test specimen

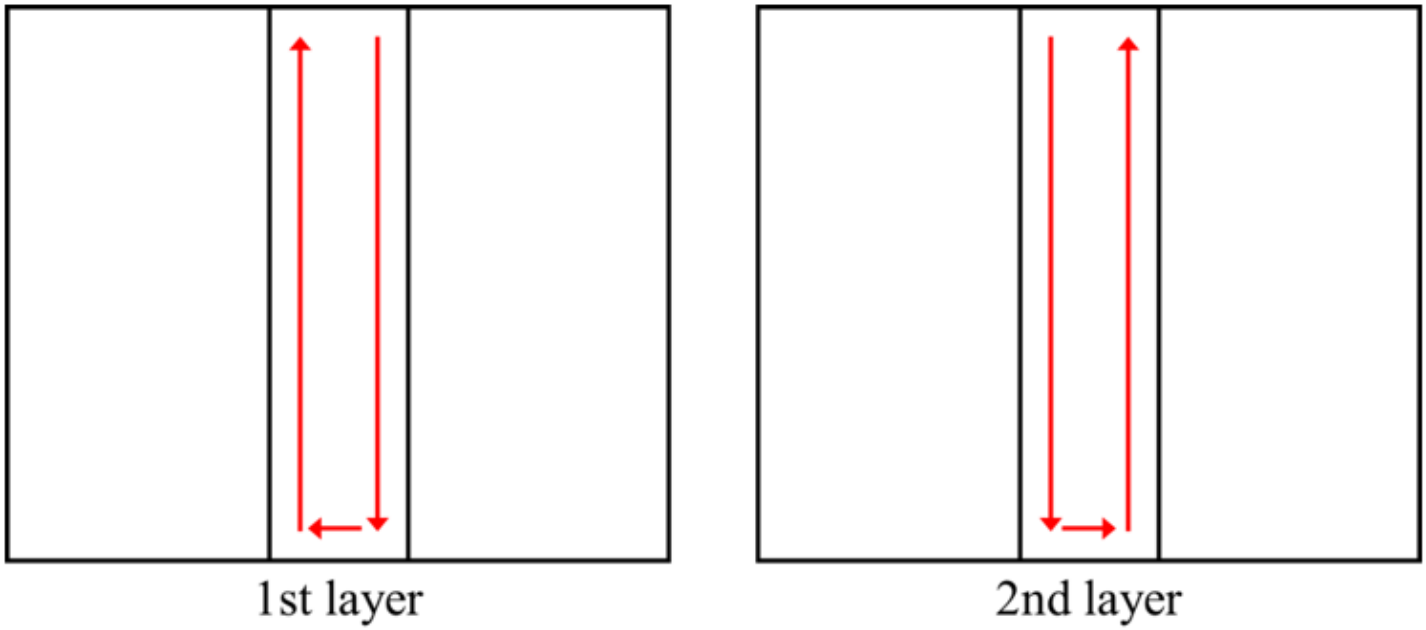

Figure 3

Deposition path used in experiments for parameter determination

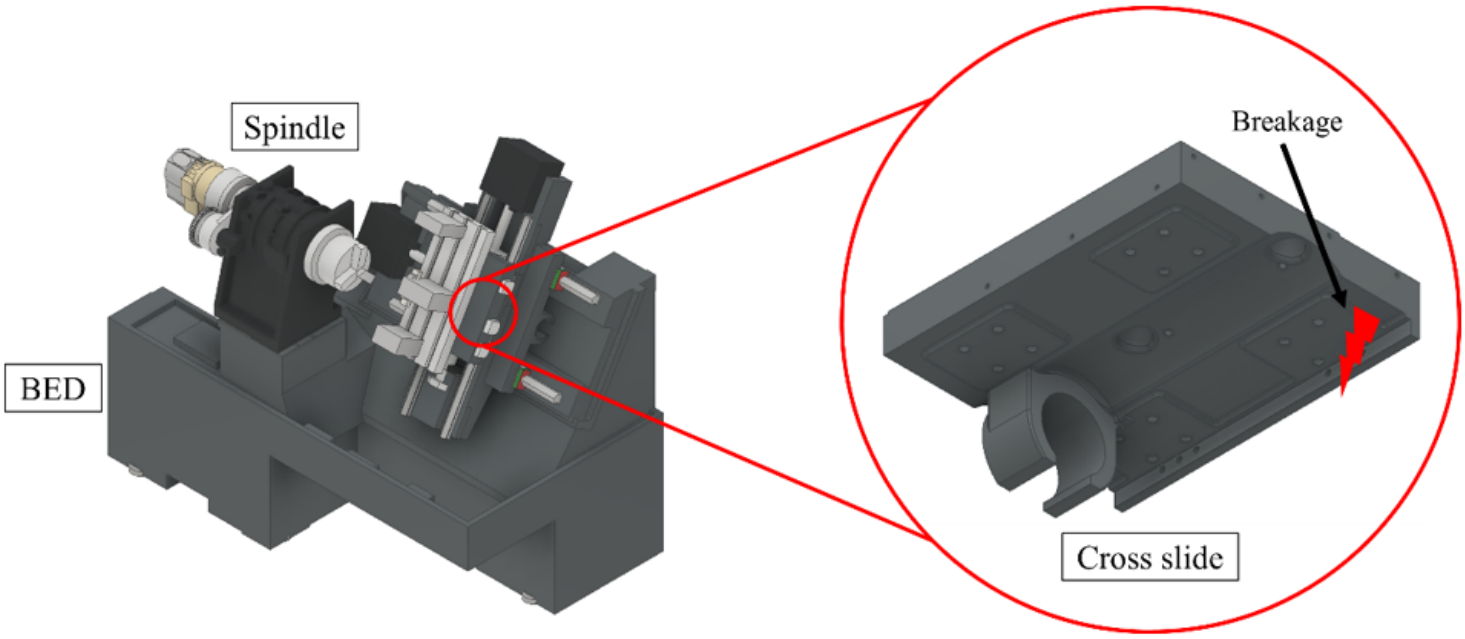

Figure 4

Example of the damaged parts in the lathe

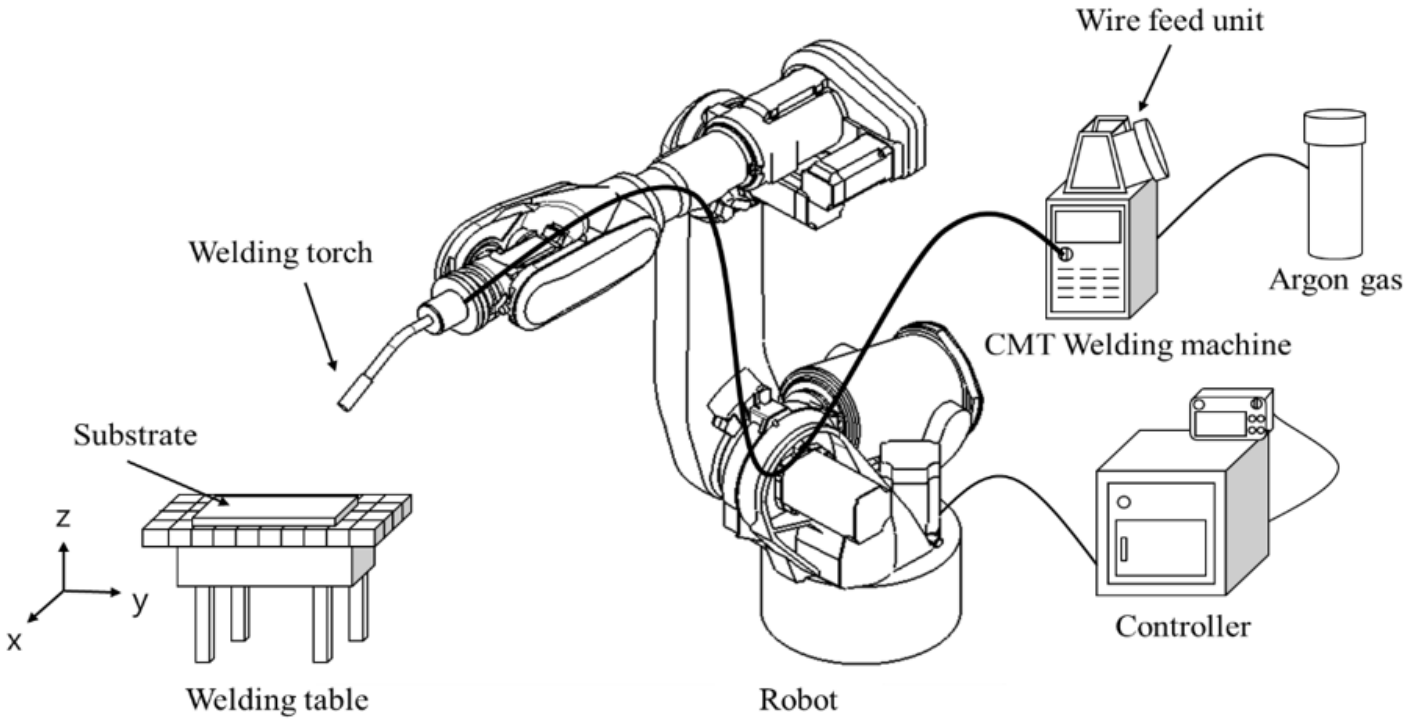

Equipment		Specification
IRB 6700 (ABB)		- Payload: 200 kg - Position repeatability: 0.05 mm - Path repeatability: 0.1–0.15 mm - Reach: 2.55–2.8 m - Weight: 1,205 kg
TPS 500i welding machine (Fronius)		- Welding current max.: 500 A - Welding current min.: 3 A - Length: 706 mm - Width: 300 mm - Height: 510 mm - Weight: 38 kg

Figure 5

Experimental setup

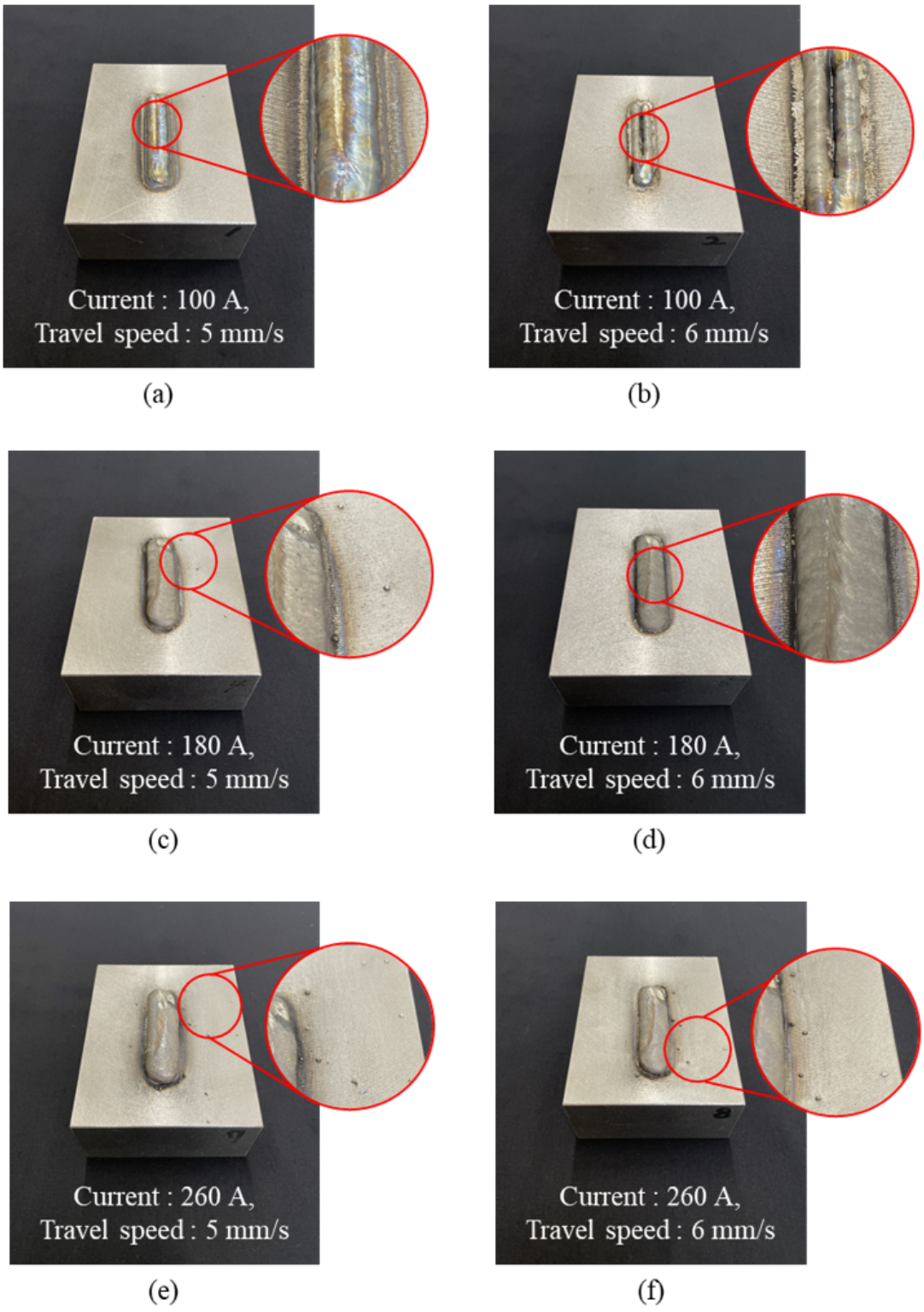

Figure 6

Results of preliminary experiments. a Current: 100 A, Travel speed: 5 mm/s, b Current: 100 A, Travel speed: 6 mm/s, c Current: 180 A, Travel speed: 5 mm/s, d Current: 180 A, Travel speed: 6 mm/s, e Current: 260 A, Travel speed: 5 mm/s, and f Current: 260 A, Travel speed: 6 mm/s

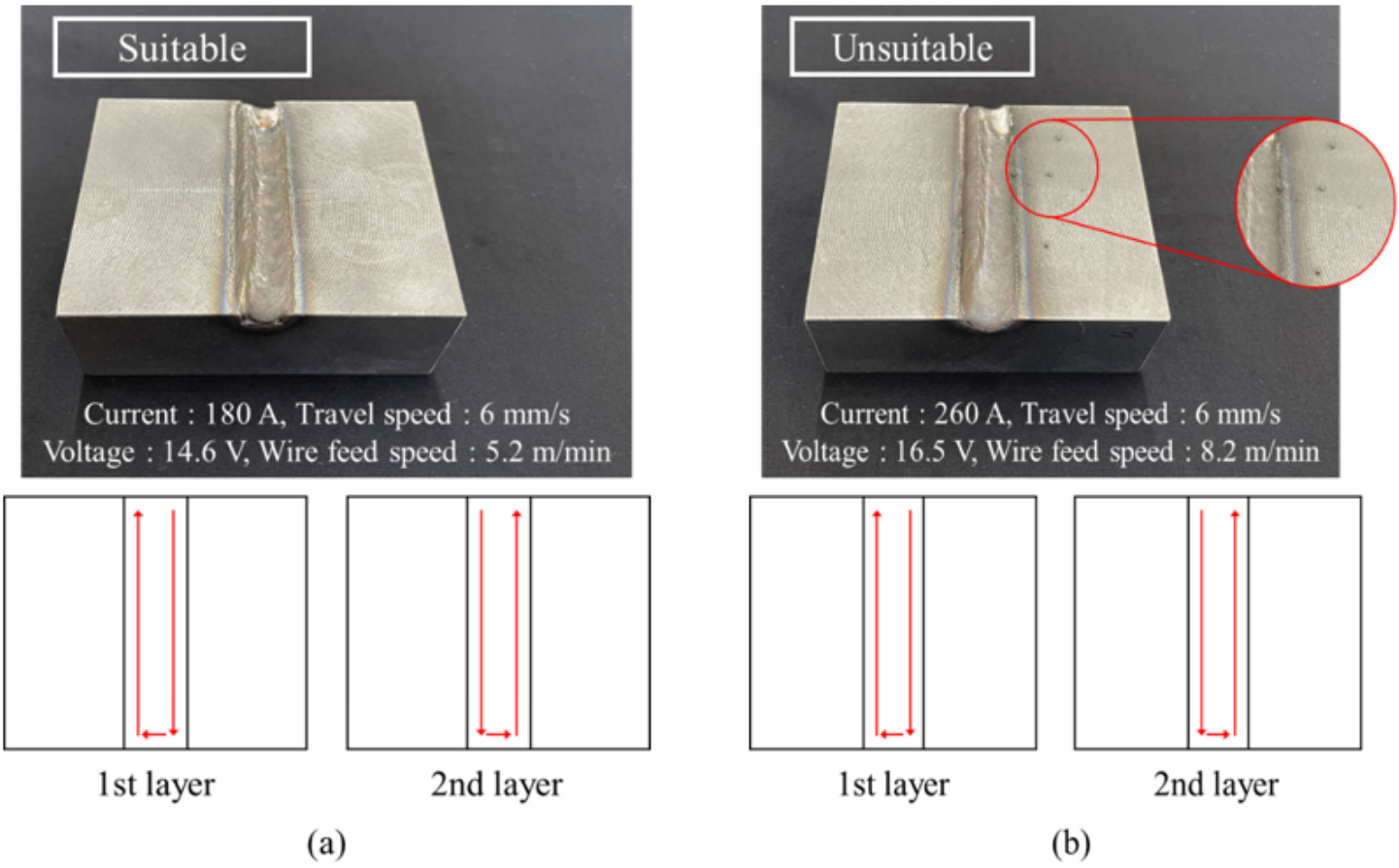

Figure 7

Repaired test specimens. a Current: 180 A, Travel speed: 6 mm/s, Voltage: 14.6 V, Wire feed speed: 5.2 m/min, and b Current: 260 A, Travel speed: 6 mm/s, Voltage: 16.5 V, Wire feed speed: 8.2 m/min

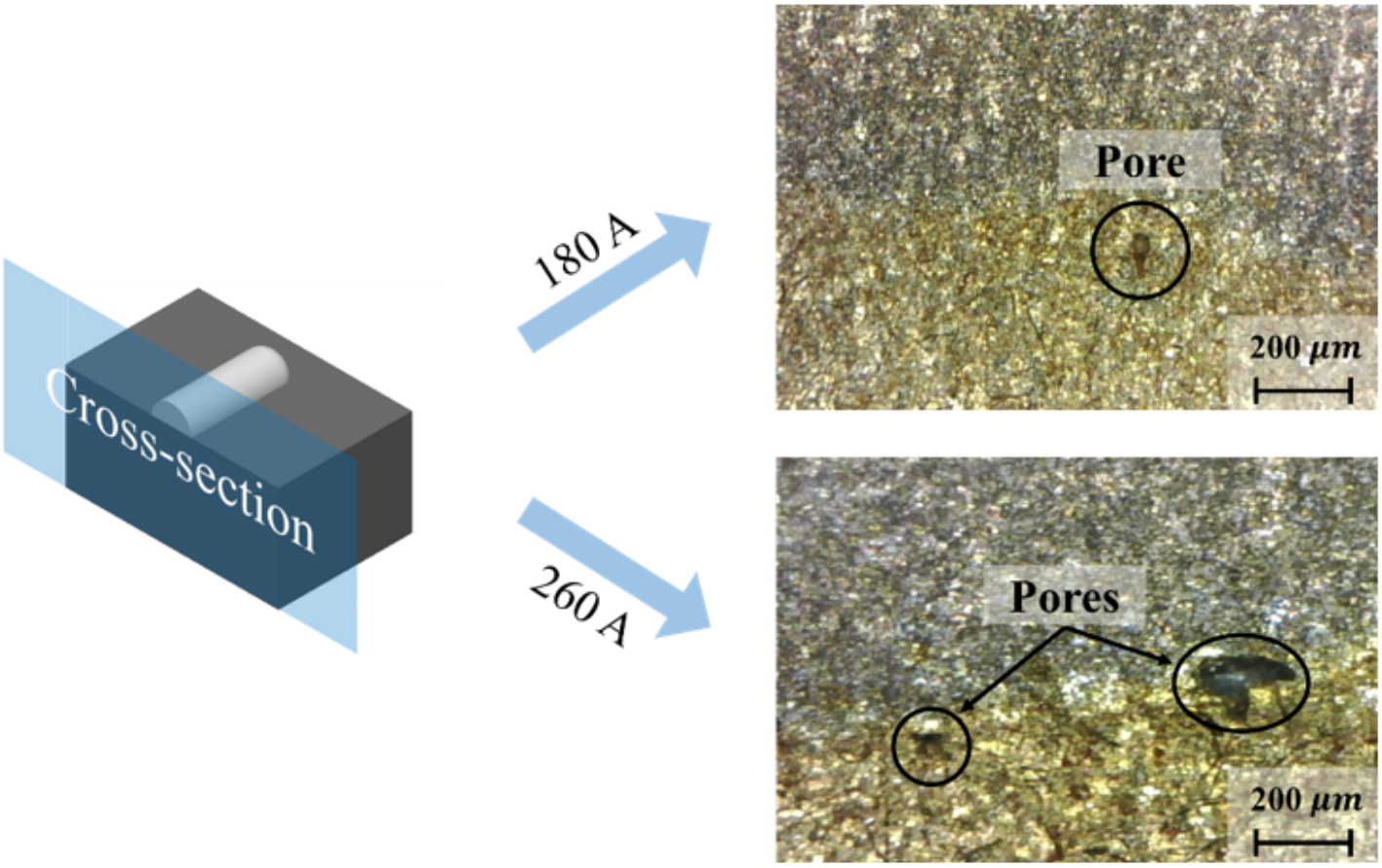

Figure 8

Results from digital microscope in preliminary experiment

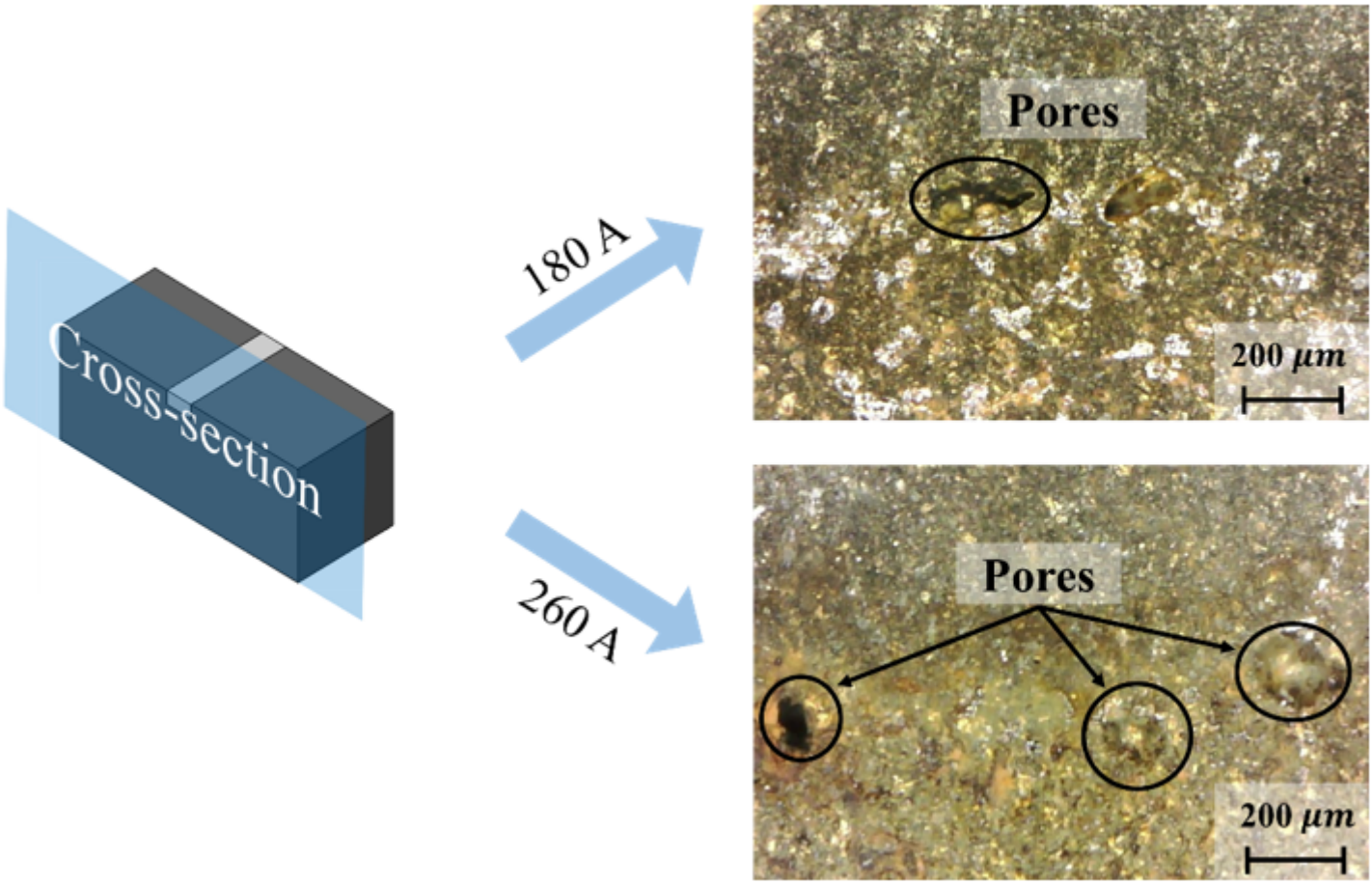

Figure 9

Results from digital microscope in repaired test specimens

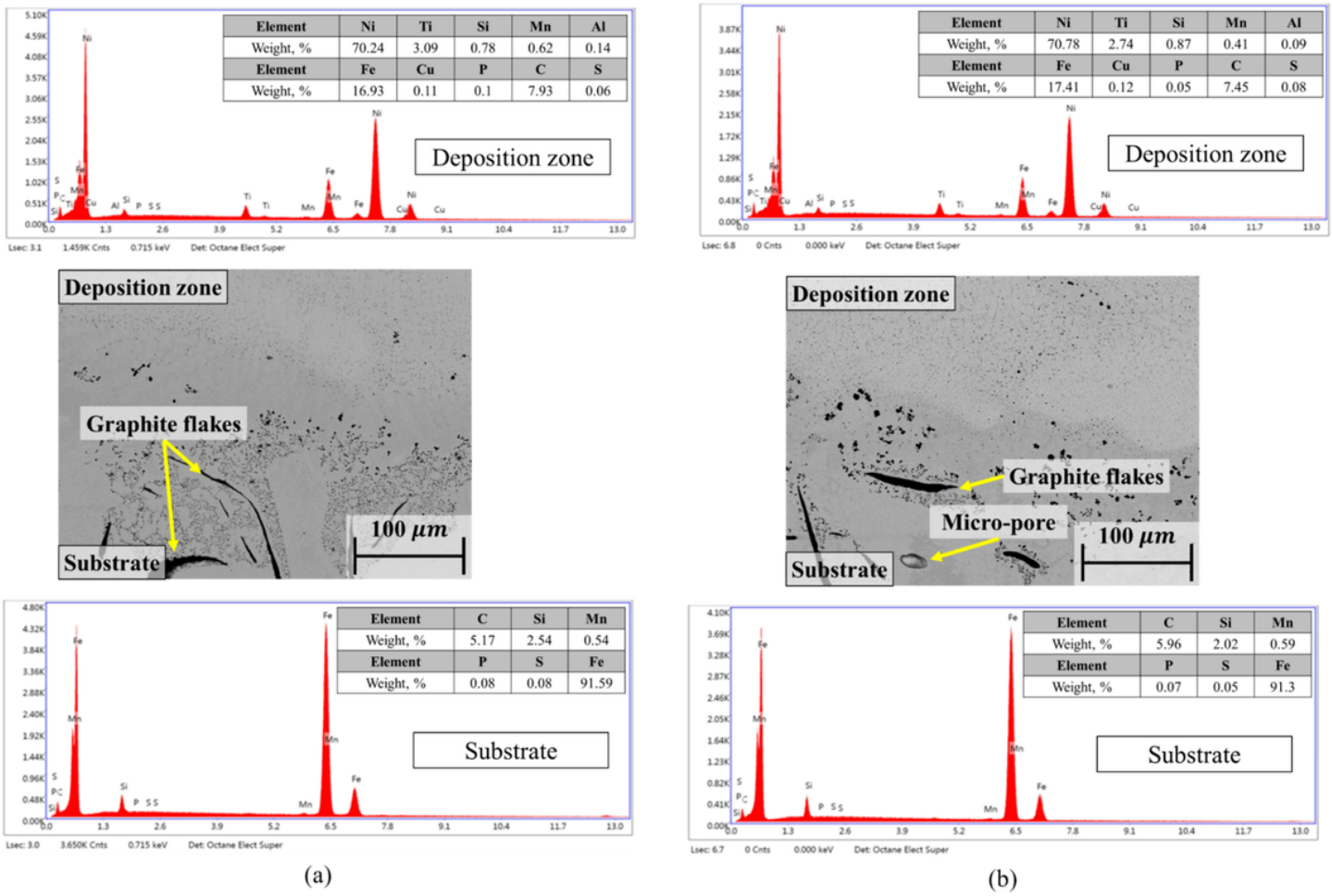

Figure 10

Results regarding microstructure and chemical composition. a Current: 180 A, Travel speed: 6 mm/s, Voltage: 14.6 V, Wire feed speed: 5.2 m/min, and b Current: 260 A, Travel speed: 6 mm/s, Voltage: 16.5 V, Wire feed speed: 8.2 m/min

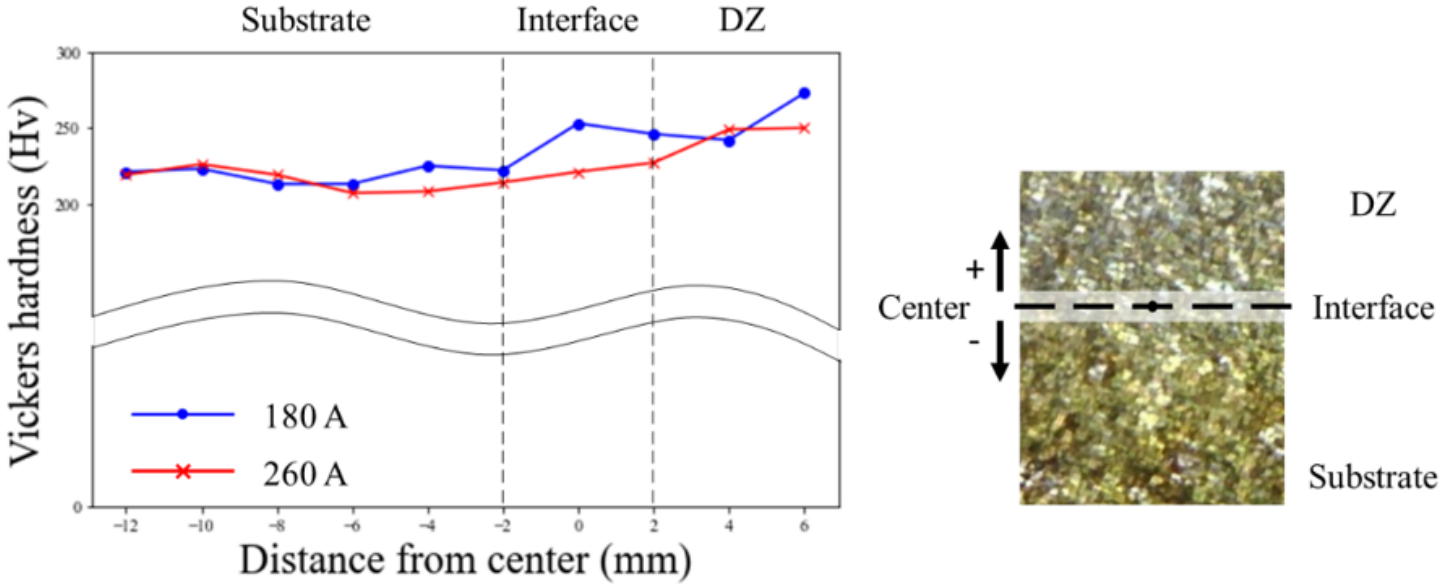

Figure 11

Results of hardness measurements

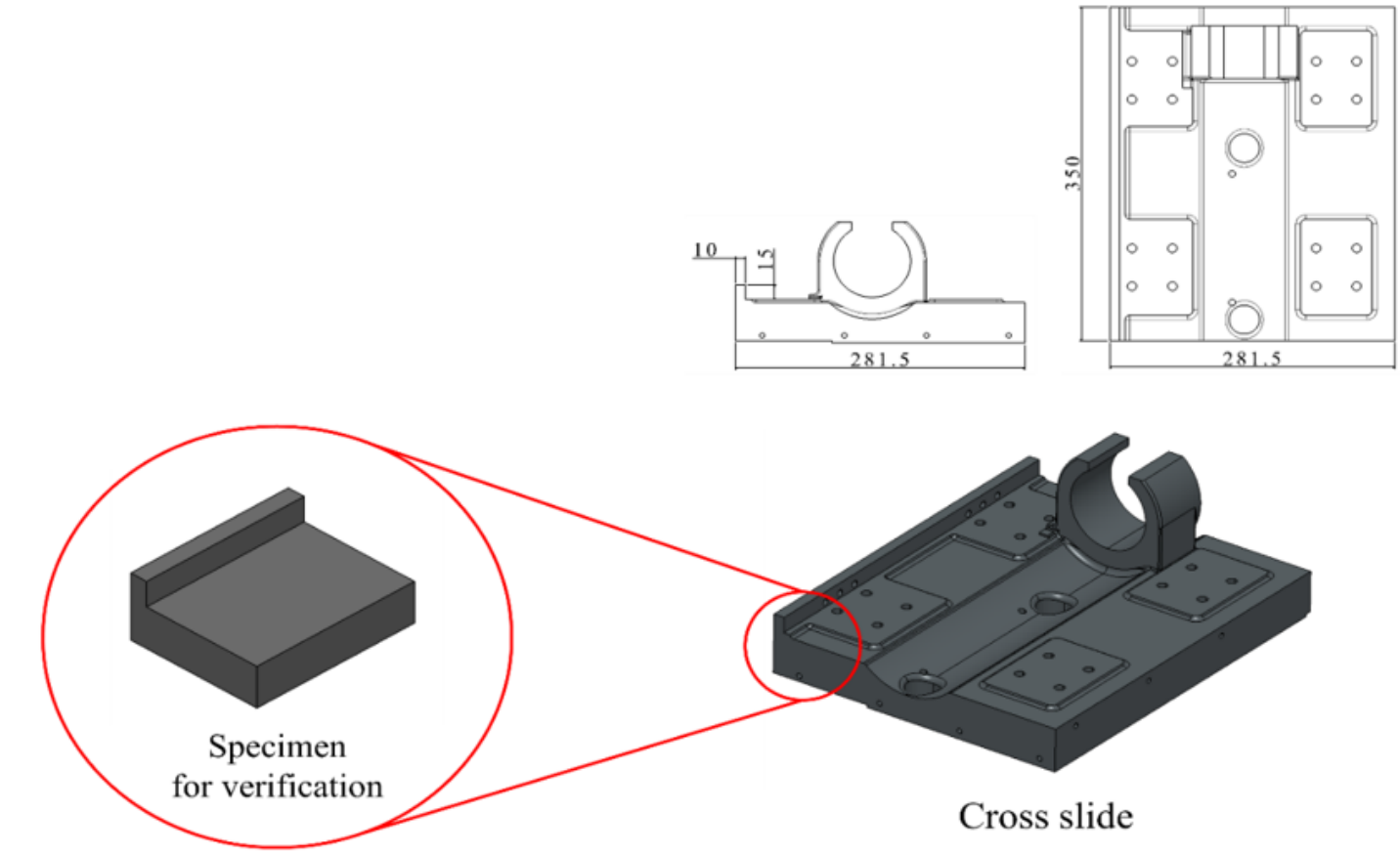

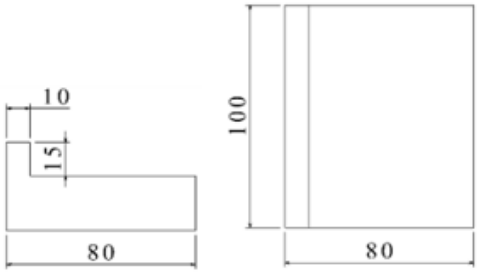

Figure 12

Schematic diagram of specimen for verification

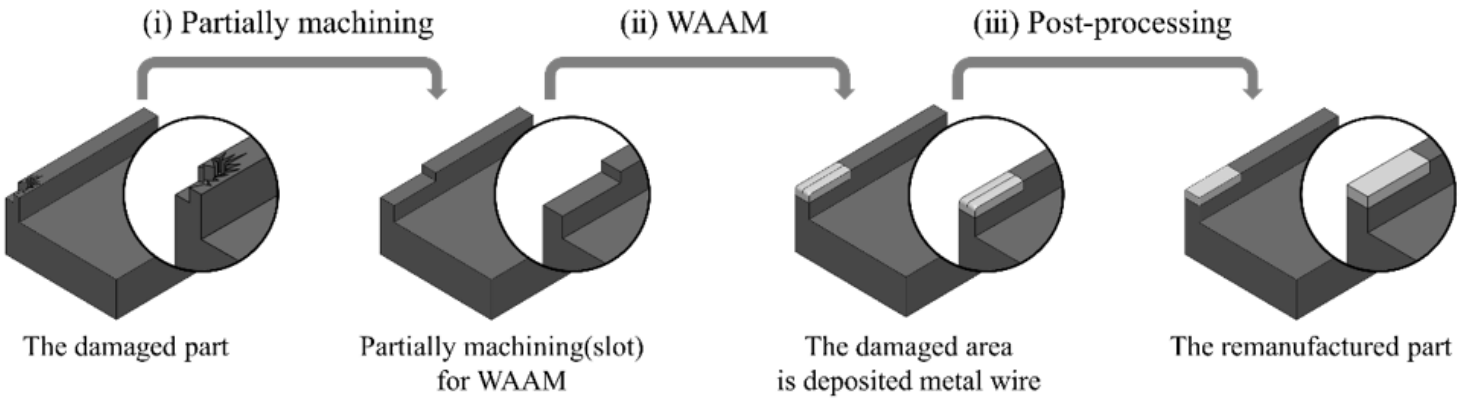

Figure 13

Repair of damaged part with surface defects using machining and wire arc additive manufacturing (WAAM)

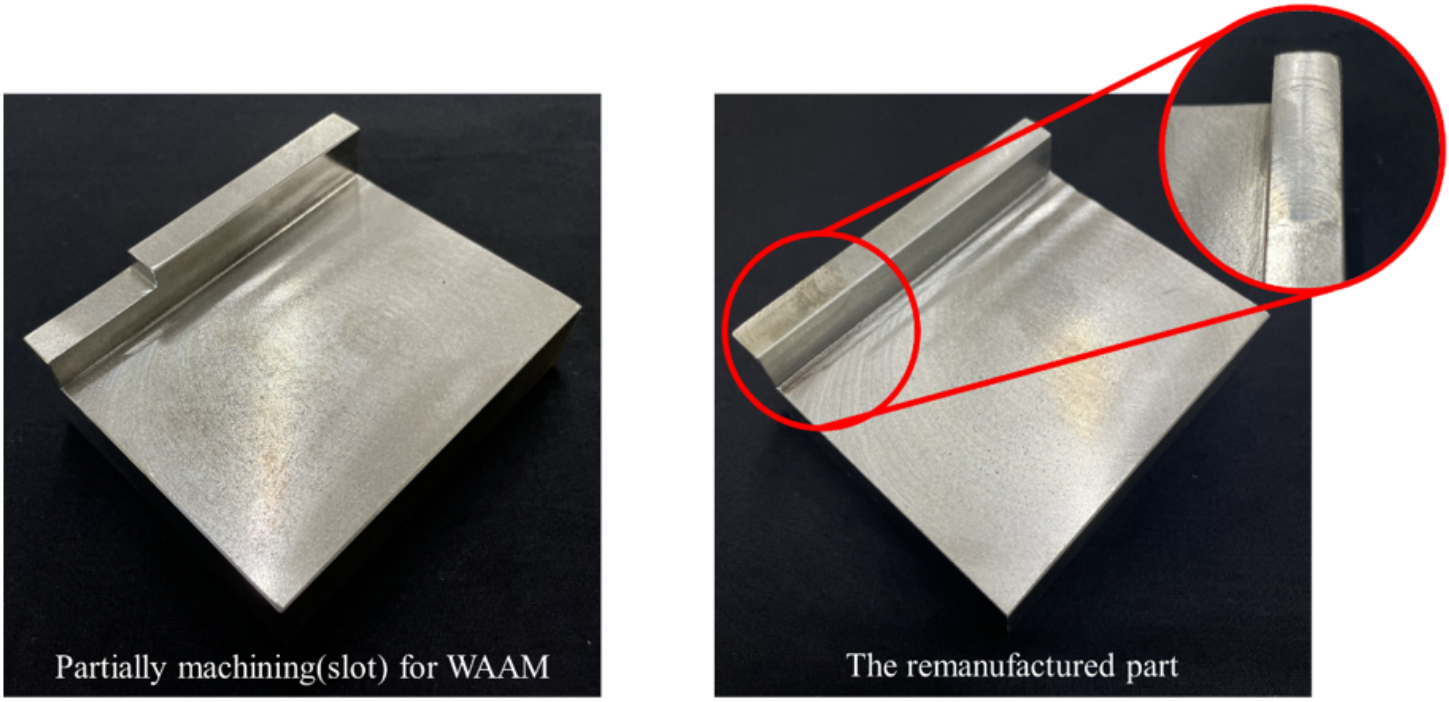

Figure 14

Results of verification experiment